

# An annular quantum gas induced by dimensional reduction on a shell

Yanliang Guo,<sup>1,\*</sup> Emmanuel Mercado Gutierrez,<sup>2</sup> David Rey,<sup>1</sup> Thomas Badr,<sup>1</sup> Aurélien Perrin,<sup>1</sup> Laurent Longchambon,<sup>1</sup> Vanderlei Salvador Bagnato,<sup>2</sup> Hélène Perrin,<sup>1</sup> and Romain Dubessy<sup>1,†</sup>

<sup>1</sup>*Université Sorbonne Paris Nord, Laboratoire de Physique des Lasers, CNRS UMR 7538, F-93430, Villetaneuse, France*

<sup>2</sup>*Instituto de Física de São Carlos, Universidade de São Paulo, CP 369, São Carlos, São Paulo, 13560-970, Brazil*

(Dated: May 28, 2021)

We report the observation of dramatic consequences of dimensional reduction onto the motional state of a quantum gas restricted to a curved two-dimensional surface. We start from the ellipsoidal geometry of a dressed quadrupole trap and introduce a novel gravity compensation mechanism enabling to explore the full ellipsoid. The dimensional reduction manifests itself by the spontaneous emergence of an annular shape in the atomic distribution, due to the zero-point energy of the transverse confinement. The experimental results are compared with the solution of the three dimensional Gross-Pitaevskii equation and with a two-dimensional semi-analytical model. This work evidences how a hidden dimension can affect dramatically the embedded low dimensional system by inducing a change of topology.

Dimensional reduction occurs when the motion of a dynamical system is constrained within a particular domain [1]. One can then construct an effective theory to describe the remaining degrees of freedom. For example the *classical* rigid pendulum oscillates in a two-dimensional (2D) plane but is described by an effective one-dimensional (1D) equation. In the *quantum* world numerous examples exploit this property to obtain new effects, as for example the realization of 1D channels [2], mesoscopic quantum devices [3] or Hall effect in 2D electron gases [4]. This phenomenon is also present in the context of high energy physics for which beyond standard model theories involve supplemental dimensions [5].

Any physical low dimensional system is still embedded in a higher dimensional space whose properties can affect the motion. For example the curvature of the constrained surface is expected to give rise to additional potential terms [1, 6, 7], while the inhomogeneity of the confining potential contributes through a slow variation of the zero-point energy [2, 7, 8].

Ultracold atom experiments offer a unique playground to probe reduced dimensions [9, 10], with many impressive achievements, as for example the simulation of the 1D Lieb-Liniger model [11], the observation of the 2D Berezinski Kosterlitz Thouless model [12, 13] or the possibility to realize synthetic dimensions [14, 15]. They recently enabled the discovery of new dynamical effects in 2D [16–18]. For interacting systems, the dimensional reduction can change the nature of interactions [19, 20] which in turn modifies the equation of state [21, 22].

In this Letter, we report the direct observation of the effect of the dimensional reduction on a gas confined to an ellipsoid surface. A novel gravity compensation mechanism enables the exploration of the full ellipsoid. We demonstrate how the motion restricted to the surface is strongly affected by a *purely quantum* effect in the frozen degree of freedom, as shown in Fig. 1. Our work illus-

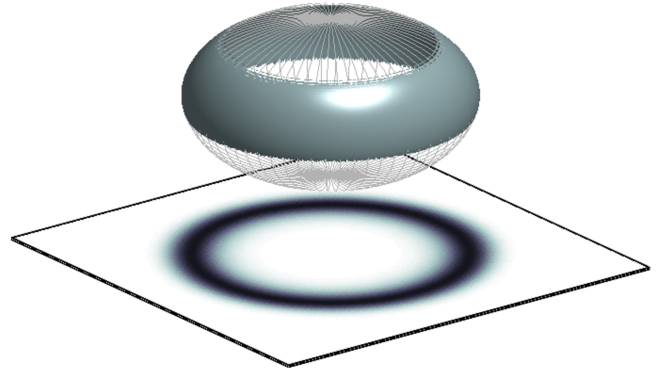


FIG. 1. Sketch of the experiment reported in this work: a quantum gas (light grey annulus) is constrained to move on a spheroidal surface (meshed surface). Because of the inhomogeneous transverse zero point energy the atoms accumulate at a given height. The shadow at the bottom shows the integrated density distribution of the gas, blurred by a  $4\text{ }\mu\text{m}$  point spread function to reproduce the experimental imaging resolution. The field of view is  $120\text{ }\mu\text{m} \times 120\text{ }\mu\text{m}$ .

trates how the inhomogeneity of the underlying three-dimensional potential can induce a dramatic change of topology in the effective two-dimensional Hamiltonian. In contrast to most experiments where it is only a small correction to the external potential, here the quantization of the transverse motion is central to the realization of an annular gas.

To constrain the motion of the atoms to a surface, we make use of adiabatic potentials realized with radio-frequency (rf) dressed ultracold atoms. They allow to access a variety of trapping geometries [23] from double wells [24–27] to bubble traps [28] and even reach the two-dimensional regime [22]. Thanks to the high degree of control on all parameters they are ideally suited to study superfluid dynamics [29–32]. By time averaging [33, 34]

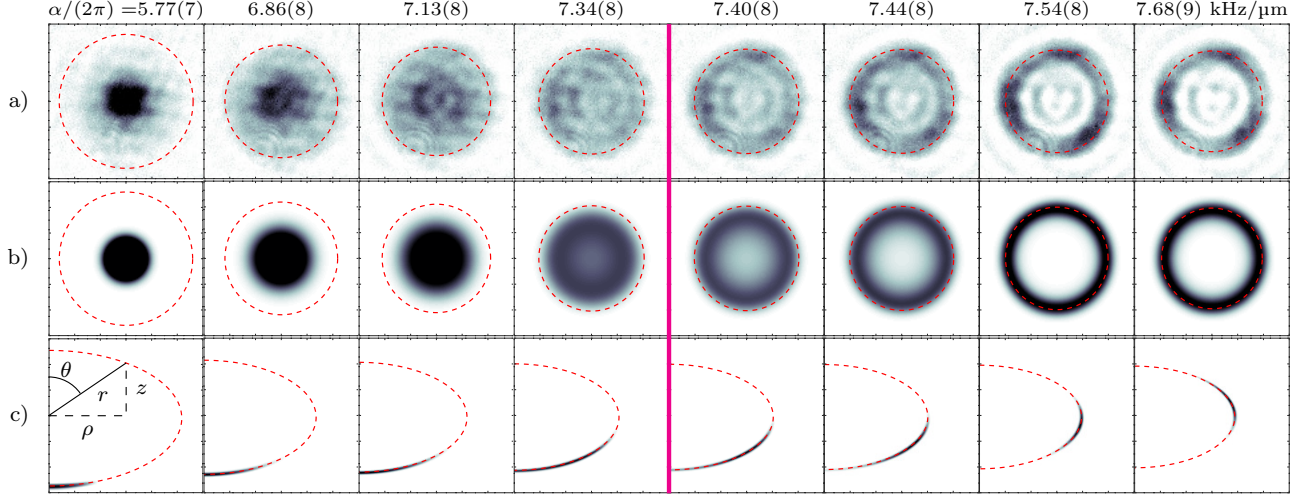


FIG. 2. (color online) In situ atomic density distribution for an ensemble of  $N \simeq 10^5$  atoms, evidencing the gravity compensation mechanism and the spontaneous change of topology, as the quadrupole gradient  $\alpha$  increases. a) experimental measurement, b) and c) full GP numerical simulation, top and side views respectively. The pink vertical line corresponds to the observed threshold for gravity compensation, slightly lower than the naive expectation  $\alpha_g/(2\pi) = 7.54(4)$  kHz/ $\mu\text{m}$ , see text for details. For each picture of a) and b) the field of view is  $120\mu\text{m} \times 120\mu\text{m}$ , the color scale spans  $[0 - 35]\mu\text{m}^{-2}$ , and the dashed circles indicate the ellipsoidal radius at equator  $\rho \equiv r_0$ . b) The simulated density profiles are convoluted with a Gaussian of  $1/\sqrt{e}$ -radius  $\sigma = 4\mu\text{m}$  to reproduce the experimental imaging resolution. For c) the field of view is  $60\mu\text{m} \times 60\mu\text{m}$  and the dashed red line is the adiabatic surface  $r = r_s(\theta)$ , see text for details.

or multiple dressing [35] even more configurations can be realized, as smooth ring-shaped waveguides [36, 37] or multiple wells [35]. Our work is also motivated by several recent studies of Bose-Einstein condensation and superfluid properties on a closed spherical surface [38–42], a configuration that is aimed at in the microgravity environment of the International Space Station using adiabatic potentials [43].

Our experimental setup is described in Ref. [22, 44]. Briefly,  $^{87}\text{Rb}$  atoms in the  $F = 1$  ground state are placed in a rotationally invariant quadrupole magnetic field of main vertical axis  $z$ . The atoms are dressed by an rf field produced by three antennas with orthogonal axes, fed by a homemade direct digital synthesis device, allowing for a full control of the rf polarization and a fine tuning of its parameters. The resulting potential, within the rotating wave approximation (RWA), reads [22]:

$$V_{3\text{D}}^{\text{RWA}}(\rho, \phi, z) = \hbar\sqrt{(\alpha\ell - \omega)^2 + \Omega(\rho, \phi, z)^2} + Mgz, \quad (1)$$

where  $\ell^2 = \rho^2 + 4z^2$ ,  $(\rho, \phi, z)$  are the usual cylindrical coordinates,  $\alpha$  is the quadrupole gradient in the horizontal plane in units of frequency,  $\omega$  is the rf frequency,  $\Omega(\rho, \phi, z)$  is the local atom-field coupling amplitude and the last term is the gravitational potential.  $\Omega(\rho, \phi, z)$  depends on the orientation of the rf polarization with respect to the local static magnetic field [45]. For the choice of a circular polarization of axis  $z$ ,  $\Omega(\rho, \phi, z) = \Omega_0/2 \times (1 - 2z/\ell)$  and the potential is rotationally invariant. Hereafter we will drop the explicit  $\phi$  dependence in all quantities. The locus of the energy minimum in

Eq. (1) belongs to a 2D ellipsoidal isomagnetic surface, defined by  $\ell = r_0 \equiv \omega/\alpha$ , slightly deformed by the gravitational sag [22]. We note that  $\Omega(\rho, z)$  reaches its maximum value  $\Omega_0$  at the bottom and vanishes at the top of this surface.

The confinement to this ellipsoid is rather strong. If we assume that the atoms are confined to the ground state of the motion transverse to the surface, we can derive an expression of the potential for the 2D motion along the ellipsoid. If we neglect the deformation of the surface due to the gravitational sag, we obtain a simple expression for the effective 2D potential:

$$V_{2\text{D}}^{\text{RWA}}(z) = \frac{\hbar\Omega_0}{2} + \left(Mg - \frac{\hbar\Omega_0}{r_0}\right)z + \frac{\hbar\omega_{\perp}(z)}{2}, \quad (2)$$

where the atoms move on the isomagnetic surface, and we have used  $\rho^2 = r_0^2 - 4z^2$ , for  $|z| \leq r_0/2$  in Eq. (1). In this expression we have neglected the geometrical effect of the curvature on the potential [1], resulting in an energy difference of order  $\hbar^2/(mr_0^2)$  between the poles and the equator, about  $\hbar \times 2$  Hz with our parameters. Equation (2) shows that the inhomogeneity in rf coupling amplitude results in a force acting against gravity. Gravity can be compensated by an appropriate choice of the magnetic field gradient, fulfilling  $\alpha_g = Mg\omega/(\hbar\Omega_0)$ . The last term in Eq. (2) involving the transverse confinement frequency  $\omega_{\perp}(z)$  is a witness of the higher dimension, entering through the zero-point energy of this degree of freedom [7, 8]. It scales as  $\alpha(z)/\sqrt{\Omega(z)}$ , where  $\alpha(z)$  and  $\Omega(z)$  are the local gradient and coupling respectively.

This quantum effect is responsible for the spontaneous change of topology when gravity is overcompensated, as shown in Fig. 2: the zero-point energy contribution to the effective potential becomes dominant as the atoms are pushed towards the top and  $\Omega(z)$  vanishes.

To demonstrate this effect we initially load the adiabatic potential with a moderate gradient  $\alpha/(2\pi) = 4.14(6)$  kHz/ $\mu\text{m}$  and a circularly polarized rf dressing field of frequency  $\omega/(2\pi) = 300$  kHz and maximum coupling amplitude  $\Omega_0/(2\pi) = 85.0(5)$  kHz. We then increase the gradient within 300 ms while keeping all the other parameters constants, and record an in-situ picture of the atomic density distribution using a standard absorption imaging scheme with the probe beam propagating along the  $z$  axis [22].

Figure 2 shows that for increasing values of the gradient  $\alpha$ , the atomic cloud expands progressively to fill the ellipsoidal surface and, when gravity is overcompensated, i.e., for  $\alpha/(2\pi) \geq 7.40(8)$  kHz/ $\mu\text{m}$ , takes a stable annular shape close to the equator. Interestingly, the compensation occurs for a gradient slightly lower than the naive expectation  $\alpha_g = 2\pi \times 7.54(4)$  kHz/ $\mu\text{m}$ . A correct modeling of the system, including beyond RWA correction to Eq. (1) and an exact description of the dimensional reduction is necessary to obtain the quantitative agreement shown in Fig. 2 between theory and simulation, as detailed below. We emphasize that the gradient  $\alpha$  and the coupling  $\Omega_0$  are calibrated with independent measurements [46] and that there is no free parameter in the simulations shown in Fig. 2.

In order to refine the theoretical description of the ring formation, we first use a Floquet (Fl) expansion [47, 48] to include beyond RWA terms. We find that even for our moderate coupling amplitude  $\Omega_0/\omega = 0.28$  it is necessary to include the first five manifolds, up to  $\pm 2$  photons, to reach convergence in the computation of the adiabatic potential  $V_{3D}^{\text{Fl}}(r, \theta)$ . Here,  $(r, \theta, \phi)$  are the spherical coordinates, see Fig. 2c, and  $V_{3D}^{\text{Fl}}$  does not depend on  $\phi$ . Using this more accurate potential, we compute numerically the mean-field atomic wave function with the Gross-Pitaevskii (GP) equation. The GP equation is propagated in imaginary time on a discrete grid to obtain the three-dimensional ground state [49]. We exploit the rotational invariance to speed up the computation and use a map to ellipsoidal coordinates to achieve good accuracy at every point of the surface [50].

Finally, we develop an improved semi-classical two-dimensional description of the potential restricted to a surface, improving the accuracy of Eq. (2). For each angle  $\theta$  we compute the potential  $V_{3D}^{\text{Fl}}(r, \theta)$  and find its minimum as a function of  $r$ , thus defining the constrained surface  $r = r_s(\theta)$ . For each point of this surface we also compute the local Hessian matrix and obtain the transverse confinement frequency  $\omega_{\perp}(\theta)$  from its largest eigen-

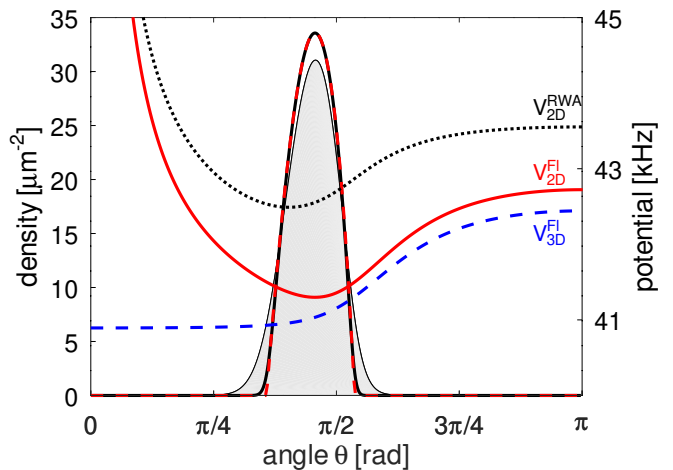


FIG. 3. (color online) Right axis: effective potential on the surface  $V_{2D}^{\text{Fl}}(\theta)$  (solid red line),  $V_{3D}^{\text{Fl}}(r_s(\theta), \theta)$  (dashed blue) and  $V_{2D}^{\text{RWA}}(z)$  (dotted black). Left axis: surface density computed with the full 3D model (grey shaded area), the 2D semi-classical model (black solid line) and 2D Thomas-Fermi solution (dashed red line). The trap parameters are:  $\omega/(2\pi) = 300$  kHz,  $\Omega_0/(2\pi) = 85.0(5)$  kHz and  $\alpha/(2\pi) = 7.68(9)$  kHz/ $\mu\text{m}$ . See text for details.

value. The improved semi-classical 2D potential reads:

$$V_{2D}^{\text{Fl}}(\theta) = V_{3D}^{\text{Fl}}(r_s(\theta), \theta) + \frac{\hbar\omega_{\perp}(\theta)}{2}. \quad (3)$$

Figure 3 evidences the difference between the quantum  $V_{2D}^{\text{Fl}}(\theta)$  and the classical  $V_{3D}^{\text{Fl}}(r_s(\theta), \theta)$  effective potentials, differing by the zero point energy contribution, see Eq. (3). Beyond RWA corrections explain the differences with the simple potential  $V_{2D}^{\text{RWA}}(z)$ , which nevertheless captures qualitatively the stabilization mechanism.

In particular, a *classical* particle evolving on the dashed blue potential curve would be pushed towards the top of the spheroid where the rf coupling vanishes, inducing Landau Zener spin flips. As a consequence, a *classical* particle can not be trapped with this configuration. The zero energy contribution provides the necessary barrier preventing the atoms to climb to the top of the ellipsoid.

With the parameters of Fig. 3, corresponding to the last column of Fig. 2, the local effective trapping frequency along the surface is  $\omega_s/(2\pi) \simeq 20$  Hz, and the transverse one varies with  $\theta$  over the cloud extent and is equal to  $\omega_{\perp}/(2\pi) = 526$  Hz at the peak density of the GP groundstate. The chemical potential of the groundstate is  $\mu/h \simeq 450$  Hz above the potential  $V_{3D}^{\text{Fl}}$  at the peak density. Therefore the quantum gas is well described by an effective two-dimensional model, with a chemical potential  $\mu_{2D} = \mu - \hbar\omega_{\perp}/2 < \hbar\omega_{\perp}$  [51]. To illustrate this point Fig. 3 compares the surface density computed with the full 3D simulation (grey shaded area) to effective 2D solutions obtained with the semi-classical potential of Eq. (3): the 2D GP solution (solid black curve) and 2D Thomas-Fermi profile (dashed red curve) [46]. Equation (3) thus

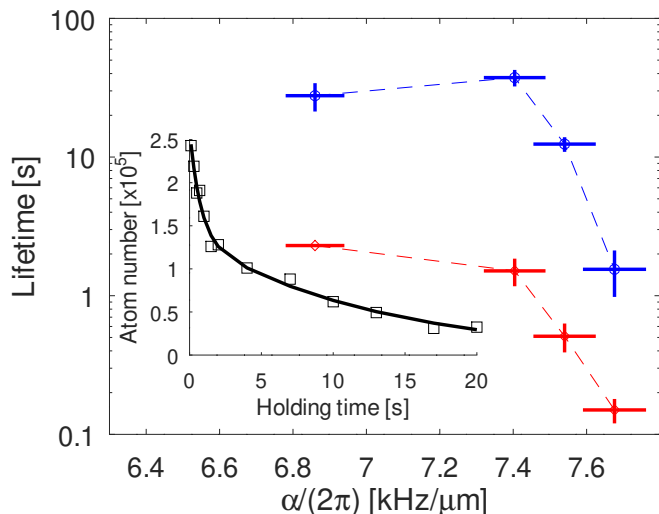


FIG. 4. (color online) Lifetime in the surface trap as a function of the quadrupole trap gradient: the blue/red symbols correspond to the two characteristic timescales, the error bars are the fit uncertainties. Inset: atom number as a function of the holding time in the trap, for a gradient of  $\alpha/(2\pi) = 7.54(8)$  kHz/ $\mu\text{m}$ , evidencing a double exponential decay. The black solid line is a fit to the data.

enables a simple and accurate description of the dimensional reduction.

When gravity is compensated, any variation of the rf amplitude of technical origin has an important effect. As a consequence, the rf polarization must be controlled with high accuracy, and the amplitudes and phases of the three antennas are optimized to the  $10^{-2}$  level. Even with our most careful rf polarization optimization we find that the annular gas presents fluctuations in the density distribution along the annulus of about 30% rms, with three apparent maxima. At the present time we do not know the origin of this long wavelength fluctuations that we estimate at the level of  $\sim \hbar \times 300$  Hz (or  $\sim 14$  nK) in chemical potential. This effect might be explained by the presence of unbalanced harmonics in the rf signal feeding the antennas and inducing extra couplings between the dressed manifolds [52].

For gradients above 7.6 kHz/ $\mu\text{m}$ , the cloud reaches regions where the rf amplitude is too low to ensure efficient rf dressing [53–55], and we observe increased Landau Zener losses and a reduced lifetime in the trap, as shown in Fig. 4. We find that the loss dynamics always follows a double exponential decay as illustrated in the inset. We note that the shortest time scale is still much longer than what we expect for three body losses that remain low for the typical peak density of  $3 \times 10^{13} \text{ cm}^{-3}$  in the experiment. Although the loss mechanism in rf dressed trap is not totally elucidated [55], we find that rings close to the equator still have a reasonable lifetime above ten seconds for our parameters.

Finally it is worth mentioning that the atoms con-

strained on the ellipsoidal surface evolve in a highly non separable potential that can not be written as a product of two harmonic oscillators. This affects the transverse excitation spectrum: the energies do not form a regular ladder, as for the harmonic oscillator. It would be interesting to study how this effect impacts the quantum gas properties: for example one can expect a modification of the usual equilibrium predictions relying on the harmonic oscillator partition function [38, 39, 41].

In conclusion we have reported an example of dimensional reduction, where the constraint induces a change of topology, resulting in an annular shaped quantum gas. We stress that the effect shown here is not due to surface curvature but to the inhomogeneous transverse confinement and is also relevant in the context of the realization of bubble shaped ensembles in microgravity using adiabatic potentials [40, 43]. We emphasize also that we have demonstrated a new method to produce a ring shaped superfluid using a particularly simple setup that does not require supplementary oscillating fields [34] nor optical potentials [56].

A consequence of this work is that the quadrupole dressed trap will spontaneously result in an annular trap geometry under microgravity environment. Once combined with the possibility to tune dynamically the rf polarization it offers an interesting platform to study rotating superfluids in anharmonic traps, on Earth or in space. For example, starting from the annular gas, one can use a small change of the rf polarization to rotate the gas [32] and then reduce the gradient to reconnect the cloud. Such protocol offers the opportunity to produce correlated states [57]. Furthermore, close to the gravity compensation setting, the harmonic confinement vanishes and the trap at the bottom of the shell has a quartic leading order, leading to new equilibrium vortex distributions in a rotating frame [58].

We acknowledge enlightening discussions with Maxim Olshanii. LPL is UMR 7538 of CNRS and Sorbonne Paris Nord University. We thank USP-COFECUB for support (project Uc Ph 177/19: Out of equilibrium trapped superfluids).

---

\* Present address: Institut für Experimentalphysik und Zentrum für Quantenphysik, Universität Innsbruck, 6020 Innsbruck, Austria

† romain.dubessy@univ-paris13.fr

- [1] R. C. T. da Costa, Quantum mechanics of a constrained particle, *Phys. Rev. A* **23**, 1982 (1981).
- [2] S. Krinner, D. Stadler, D. Husmann, J.-P. Brantut, and T. Esslinger, Observation of quantized conductance in neutral matter, *Nature* **517**, 64 (2015).
- [3] Y. Imry, Mesoscopic Physics and the Fundamentals of Quantum Mechanics, *Physica Scripta* **T76**, 171 (1998), 9807306.
- [4] E. H. Hall, On a New Action of the Magnet on Elec-



- tric Currents, *American Journal of Mathematics* **2**, 287 (1879).
- [5] L. Randall and R. Sundrum, Large Mass Hierarchy from a Small Extra Dimension, *Phys. Rev. Lett.* **83**, 3370 (1999).
  - [6] L. Kaplan, N. T. Maitra, and E. J. Heller, Quantizing constrained systems, *Phys. Rev. A* **56**, 2592 (1997).
  - [7] P. Sandin, M. Ögren, M. Gulliksson, J. Smyrnakis, M. Magiropoulos, and G. M. Kavoulakis, Dimensional reduction in Bose-Einstein condensed clouds of atoms confined in tight potentials of any geometry and any interaction strength, *Phys. Rev. E* **95**, 012142 (2017).
  - [8] S. Schwartz, M. Cozzini, C. Menotti, I. Carusotto, P. Bouyer, and S. Stringari, One-dimensional description of a Bose-Einstein condensate in a rotating closed-loop waveguide, *New J. Phys.* **8**, 162 (2006).
  - [9] A. Görlitz, J. M. Vogels, a. E. Leanhardt, C. Raman, T. L. Gustavson, J. R. Abo-Shaeer, a. P. Chikkatur, S. Gupta, S. Inouye, T. Rosenband, and W. Ketterle, Realization of Bose-Einstein condensates in lower dimensions, *Phys. Rev. Lett.* **87**, 130402 (2001).
  - [10] L. Pricoupenko, H. Perrin, and M. Olshanii, eds., *Quantum Gases in Low Dimensions*, Vol. 116 (J. Phys. IV France, 2004).
  - [11] T. Kinoshita, T. Wenger, and D. S. Weiss, A quantum Newton's cradle, *Nature* **440**, 900 (2006).
  - [12] Z. Hadzibabic, P. Krüger, M. Cheneau, B. Battelier, and J. Dalibard, Berezinskii-Kosterlitz-Thouless crossover in a trapped atomic gas, *Nature* **441**, 1118 (2006).
  - [13] R. J. Fletcher, M. Robert-de Saint-Vincent, J. Man, N. Navon, R. P. Smith, K. G. H. Viebahn, and Z. Hadzibabic, Connecting Berezinskii-Kosterlitz-Thouless and BEC Phase Transitions by Tuning Interactions in a Trapped Gas, *Phys. Rev. Lett.* **114**, 255302 (2015).
  - [14] M. Mancini, G. Pagano, G. Cappellini, L. Livì, M. Rider, J. Catani, C. Sias, P. Zoller, M. Inguscio, M. Dalmonte, and L. Fallani, Observation of chiral edge states with neutral fermions in synthetic hall ribbons, *Science* **349**, 1510 (2015).
  - [15] T. Chalopin, T. Satoor, A. Evrard, V. Makhalov, J. Dalibard, R. Lopes, and S. Nascimbene, Probing chiral edge dynamics and bulk topology of a synthetic Hall system, *Nat. Phys.* **16**, 1017 (2020).
  - [16] R. Saint-Jalm, P. C. Castilho, Le Cerf, B. Bakka-Hassani, J. L. Ville, S. Nascimbene, J. Beugnon, and J. Dalibard, Dynamical Symmetry and Breathers in a Two-Dimensional Bose Gas, *Phys. Rev. X* **9**, 21035 (2019).
  - [17] Z.-Y. Shi, C. Gao, and H. Zhai, Idealized hydrodynamics (2020), arXiv:2011.01415 [cond-mat.quant-gas].
  - [18] M. Olshanii, D. Deshommes, J. Torrents, M. Gonchenko, V. Dunjko, and G. E. Astrakharchik, Triangular Gross-Pitaevskii breathers and Damski-Chandrasekhar shock waves (2021), arXiv:2102.12184 [cond-mat.quant-gas].
  - [19] M. Olshanii, Atomic Scattering in the Presence of an External Confinement and a Gas of Impenetrable Bosons, *Phys. Rev. Lett.* **81**, 938 (1998).
  - [20] M. Olshanii, H. Perrin, and V. Lorent, Example of a Quantum Anomaly in the Physics of Ultracold Gases, *Phys. Rev. Lett.* **105**, 095302 (2010).
  - [21] C.-L. Hung, X. Zhang, N. Gemelke, and C. Chin, Observation of scale invariance and universality in two-dimensional Bose gases, *Nature* **470**, 236 (2011).
  - [22] K. Merloti, R. Dubessy, L. Longchambon, A. Perrin, P.-E. P.-E. Pottier, V. Lorent, and H. Perrin, A two-dimensional quantum gas in a magnetic trap, *New J. Phys.* **15**, 033007 (2013).
  - [23] B. M. Garraway and H. Perrin, Recent developments in trapping and manipulation of atoms with adiabatic potentials, *J. Phys. B* **49**, 172001 (2016).
  - [24] T. Schumm, S. Hofferberth, L. M. Andersson, S. Wildermuth, S. Groth, I. Bar-Joseph, J. Schmiedmayer, and P. Krüger, Matter wave interferometry in a double well on an atom chip, *Nat. Phys.* **1**, 57 (2005).
  - [25] S. Hofferberth, I. Lesanovsky, B. Fischer, J. Verdu, and J. Schmiedmayer, Radiofrequency-dressed-state potentials for neutral atoms, *Nat. Phys.* **2**, 710 (2006).
  - [26] I. Lesanovsky, T. Schumm, S. Hofferberth, L. M. Andersson, P. Krüger, and J. Schmiedmayer, Adiabatic radio-frequency potentials for the coherent manipulation of matter waves, *Phys. Rev. A* **73**, 033619 (2006).
  - [27] A. J. Barker, S. Sunami, D. Garrick, A. Beregi, K. Luksch, E. Bentine, and C. J. Foot, Coherent splitting of two-dimensional Bose gases in magnetic potentials, *New J. Phys.* **22**, 103040 (2020).
  - [28] Y. Colombe, E. Knyazchyan, O. Morizot, B. Mercier, V. Lorent, and H. Perrin, Ultracold atoms confined in rf-induced two-dimensional trapping potentials, *Eur. Phys. Lett.* **67**, 593 (2004).
  - [29] K. Merloti, R. Dubessy, L. Longchambon, M. Olshanii, and H. Perrin, Breakdown of scale invariance in a quasi-two-dimensional Bose gas due to the presence of the third dimension, *Phys. Rev. A* **88**, 061603 (2013).
  - [30] R. Dubessy, C. De Rossi, T. Badr, L. Longchambon, and H. Perrin, Imaging the collective excitations of an ultracold gas using statistical correlations, *New J. Phys.* **16**, 122001 (2014).
  - [31] C. De Rossi, R. Dubessy, K. Merloti, M. De Goër de Herve, T. Badr, A. Perrin, L. Longchambon, and H. Perrin, Probing superfluidity in a quasi two-dimensional Bose gas through its local dynamics, *New J. Phys.* **18**, 062001 (2016).
  - [32] Y. Guo, R. Dubessy, M. De Goër de Herve, A. Kumar, T. Badr, A. Perrin, L. Longchambon, and H. Perrin, Supersonic Rotation of a Superfluid: A Long-Lived Dynamical Ring, *Phys. Rev. Lett.* **124**, 025301 (2020).
  - [33] I. Lesanovsky and W. Von Klitzing, Time-averaged adiabatic potentials: Versatile matter-wave guides and atom traps, *Phys. Rev. Lett.* **99**, 083001 (2007).
  - [34] B. E. Sherlock, M. Gildemeister, E. Owen, E. Nugent, and C. J. Foot, Time-averaged adiabatic ring potential for ultracold atoms, *Phys. Rev. A* **83**, 043408 (2011).
  - [35] T. L. Harte, E. Bentine, K. Luksch, A. J. Barker, D. Trypogeorgos, B. Yuen, and C. J. Foot, Ultracold atoms in multiple radio-frequency dressed adiabatic potentials, *Phys. Rev. A* **97**, 013616 (2018).
  - [36] P. Navez, S. Pandey, H. Mas, K. Poullos, T. Fernholz, and W. von Klitzing, Matter-wave interferometers using TAAP rings, *New J. Phys.* **18**, 075014 (2016).
  - [37] S. Pandey, H. Mas, G. Drougakis, P. Thekkepatt, V. Bolpasi, G. Vasilakis, K. Poullos, and W. von Klitzing, Hypersonic Bose-Einstein condensates in accelerator rings, *Nature* **570**, 205 (2019).
  - [38] S. J. Bereta, L. Madeira, V. S. Bagnato, and M. A. Caracanhas, Bose-Einstein condensation in spherically symmetric traps, *Am. J. Phys.* **87**, 924 (2019).
  - [39] A. Tononi and L. Salasnich, Bose-Einstein Condensation

- on the Surface of a Sphere, *Phys. Rev. Lett.* **123**, 160403 (2019).
- [40] A. Tononi, F. Cinti, and L. Salasnich, Quantum Bubbles in Microgravity, *Phys. Rev. Lett.* **125**, 010402 (2020).
  - [41] N. S. Möller, F. E. A. dos Santos, V. S. Bagnato, and A. Pelster, Bose–Einstein condensation on curved manifolds, *New Journal of Physics* **22**, 063059 (2020).
  - [42] S. J. Bereta, M. A. Caracanhas, and A. L. Fetter, Superfluid vortex dynamics on a spherical film, *Phys. Rev. A* **103**, 053306 (2021).
  - [43] N. Lundblad, R. A. Carollo, C. Lannert, M. J. Gold, X. Jiang, D. Paseltiner, N. Sergay, and D. C. Aveline, Shell potentials for microgravity Bose-Einstein condensates, *npj Microgravity* **5**, 30 (2019).
  - [44] R. Dubessy, K. Merloti, L. Longchambon, P.-E. Pottier, T. Liennard, A. Perrin, V. Lorent, and H. Perrin, Rubidium-87 Bose-Einstein condensate in an optically plugged quadrupole trap, *Phys. Rev. A* **85**, 013643 (2012).
  - [45] H. Perrin and B. M. Garraway, Chapter four - trapping atoms with radio frequency adiabatic potentials (Academic Press, 2017) pp. 181–262.
  - [46] See Supplemental Material at [URL will be inserted by publisher] for details on the fine control of the dressed trap, calibration procedures and a formal description of the dimensional reduction.
  - [47] J. H. Shirley, Solution of the schrödinger equation with a hamiltonian periodic in time, *Phys. Rev.* **138**, B979 (1965).
  - [48] S. Hofferberth, B. Fischer, T. Schumm, J. Schmiedmayer, and I. Lesanovsky, Ultracold atoms in radio-frequency dressed potentials beyond the rotating-wave approximation, *Phys. Rev. A* **76**, 013401 (2007).
  - [49] X. Antoine, C. Besse, R. Duboscq, and V. Rispoli, Acceleration of the imaginary time method for spectrally computing the stationary states of Gross–Pitaevskii equations, *Comput. Phys. Commun.* **219**, 70 (2017).
  - [50] The details will be published elsewhere.
  - [51] D. S. Petrov, M. Holzmann, and G. V. Shlyapnikov, Bose-Einstein Condensation in Quasi-2D Trapped Gases, *Phys. Rev. Lett.* **84**, 2551 (2000).
  - [52] We have verified that the amplitude of all harmonics are at least 20 dB below the fundamental component.
  - [53] O. Zobay and B. M. Garraway, Two-dimensional atom trapping in field-induced adiabatic potentials, *Phys. Rev. Lett.* **86**, 1195 (2001).
  - [54] O. Zobay and B. M. Garraway, Atom trapping and two-dimensional Bose-Einstein condensates in field-induced adiabatic potentials, *Phys. Rev. A* **69**, 023605 (2004).
  - [55] K. A. Burrows, H. Perrin, and B. M. Garraway, Nonadiabatic losses from radio-frequency-dressed cold-atom traps: Beyond the landau-zener model, *Phys. Rev. A* **96**, 023429 (2017).
  - [56] W. H. Heathcote, E. Nugent, B. T. Sheard, and C. J. Foot, A ring trap for ultracold atoms in an RF-dressed state, *New J. Phys.* **10**, 043012 (2008).
  - [57] M. Roncaglia, M. Rizzi, and J. Dalibard, From rotating atomic rings to quantum Hall states, *Sci. Rep.* **1**, 1 (2011).
  - [58] L. Brito, A. Andriati, L. Tomio, and A. Gamal, Breakup of rotating asymmetric quartic-quadratic trapped condensates, *Phys. Rev. A* **102**, 063330 (2020).
  - [59] R. K. Easwaran, L. Longchambon, P.-E. Pottier, V. Lorent, H. Perrin, and B. M. Garraway, RF spectroscopy in a resonant RF-dressed trap, *J. Phys. B* **43**, 065302 (2010).

## SUPPLEMENTAL MATERIAL

*Static magnetic field control* In order to calibrate precisely the gradient of the quadrupole coils, we measure the vertical displacement of the cloud in the dressed quadrupole trap as a function of the dressing frequency  $\omega$ , from 300 kHz to 3 MHz and from a linear fit we extract directly the gradient in units of kHz/ $\mu\text{m}$ . We load the trap with a reduced coupling  $\Omega_0/(2\pi) \simeq 40$  kHz such that the atoms are always at the bottom of the ellipsoid, and measure the vertical position of the atoms after a 23 ms time-of-flight using an additional imaging axis along an horizontal direction. An ensemble of large coils along three orthogonal axis allows to cancel the static homogeneous magnetic field at the position of the atoms: therefore the center of mass of the cloud is not displaced in the horizontal plane when the gradient changes. We repeat this procedure for different gradients in the range 4.14(6) to 8.49(9) kHz/ $\mu\text{m}$  covering all the data presented in this work and achieve a relative uncertainty of one percent. The experimental values of the gradient given in the main text result from a linear interpolation at any gradient between the measured points.

*Radio-frequency spectroscopy* To determine precisely the radio-frequency coupling amplitude we perform radio-frequency spectroscopy [48, 59]: using a weak additional rf field, produced by an antenna aligned with the vertical axis, we probe the energy difference between the dressed states at the position of the atoms. When the frequency is resonant this probe field induces losses that are recorded after typically 500 ms of weak rf probe pulse. We repeat this measurement for various probe frequencies and record a loss spectrum. At low gradient the resonant frequency is always larger than the effective coupling due to the gravitational sag. A careful comparison with the simulated density distribution is necessary to accurately infer the coupling amplitude. We find  $\Omega_0 = 2\pi \times 85.0(5)$  kHz, see Fig. S1.

For larger gradients, when gravity is overcompensated and the atoms climb on the surface, the local energy difference between dressed states is reduced. As shown in Fig. S1 this results in a reduction of the resonant frequency and a broadening of the spectrum. The zero-temperature GP simulation captures both effects. Furthermore small variations of the simulation parameters ( $\Omega_0$  or  $\alpha$ ) result in noticeable changes of the simulated distribution, allowing us to estimate the uncertainty on the rf coupling amplitude at the level of  $\pm 0.5$  kHz. We note however that several systematic effects can affect this comparison: the experiment is done at small but finite temperature, while the simulation assumes zero temperature, and the spectroscopic signal depends also on the probe polarization, which is not modeled.

*Fine tuning of the rf polarization* The measurements reported in Fig. 2 and the comparison with numerical

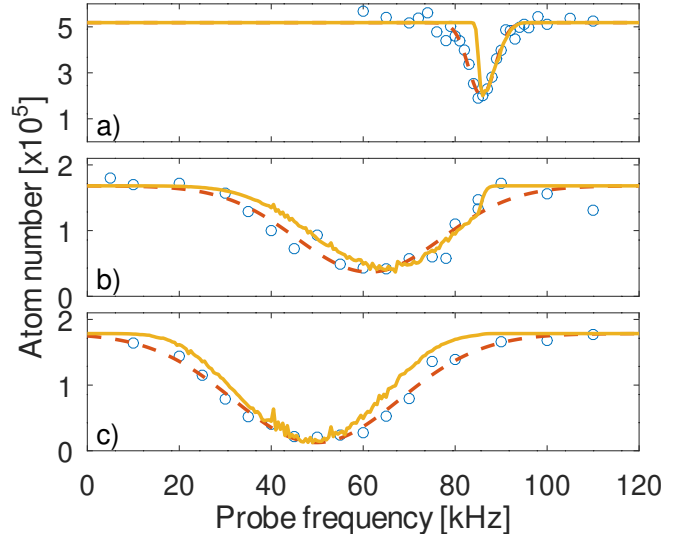


FIG. S1. (Color online) rf spectroscopy signal: atom number as a function of the rf probe frequency (open blue circles), gaussian fit to the data (dashed red curve) and simulation (solid yellow curve). The trap parameters are  $\omega = 2\pi \times 300$  kHz,  $\Omega_0 = 2\pi \times 85.0(5)$  kHz and  $\alpha = 2\pi \times \{4.14, 7.40, 7.54\}$  kHz/ $\mu\text{m}$  for a), b) and c) respectively.

simulations assume a perfectly circularly polarized rf field (with respect to the  $z$  axis). To achieve this we control the amplitude and the phase of the signals fed to the three dressing antennas. We find that the most sensitive configuration to finely tune the polarization is the over compensated ring trap: any imbalance in the polarization results in density inhomogeneities along the ring. The optimization procedure proceeds as follows: we first roughly equilibrate the amplitudes of the two horizontal plane antennas with a dephasing of  $\delta\Phi \sim \pi/2$ . This usually results in an inhomogeneous ring with two local density maxima. We then tune the third, vertical axis antenna to balance the atom number between the two maxima by tuning its amplitude  $A_z$  and change their relative position on the ring by controlling its phase  $\phi_z$ , such that we obtain two opposite maxima along one diameter of the ring. Now changing  $\delta\Phi$  results in a simultaneous rotation of the two maxima along by some angle  $\phi_0(\delta\Phi)$ . We observe that  $\phi_0(\delta\Phi) \sim \arctan[(\delta\Phi - \delta\Phi_{\text{opt}})/\sigma_\Phi]/2$  where  $\delta\Phi_{\text{opt}}$  is the optimal phase difference and the width  $\sigma_\Phi$  is minimized when the amplitudes of the two horizontal antennas are perfectly balanced. After a few iterations we obtain an almost homogeneous atomic ring, as shown in Fig. 2.

*In situ imaging* We use a homemade four lenses imaging objective attached to the camera. The depth of view is about 100  $\mu\text{m}$ , larger than the vertical distance traveled by the atoms in the picture series of Fig. 2. The resolution is 4  $\mu\text{m}$  (Rayleigh criterion), limited by the numerical aperture  $\sim 0.1$ . After alignment and focus adjustment using a triaxial translation stage, we take several pictures

of a small cloud at the bottom of the trap while moving the imaging system along an horizontal axis. From a fit of the center of mass of the cloud position as a function of the displacement, measured on the translation stage, we obtain a magnification of 7.78.

*Dimensional reduction* We provide here a short summary of dimensional reduction on a surface [1, 6–8], adapted to the geometry of the experiment reported in the main text. The full mathematical derivation will be discussed elsewhere and we focus only on the key ingredients. In particular we have verified that the contribution of the surface curvature itself is small compared to the inhomogeneous transverse confinement and does not play a key role. Therefore we start by recalling that the mean field groundstate is found by solving the three-dimensional Gross-Pitaevskii (GP) equation:

$$\mu\psi = \left(-\frac{\hbar^2}{2M}\Delta + V(\mathbf{r}) + g|\psi|^2\right)\psi,$$

where the wavefunction  $\psi \equiv \psi(\mathbf{r})$  is normalized to the number of particles:  $N = \int d^3\mathbf{r} |\psi|^2$ ,  $\mu$  is the chemical potential,  $M$  is the atomic mass, and  $g = 4\pi a_s \hbar^2 / M$  is the two-body interaction strength, with  $a_s$  the low energy  $s$ -wave scattering length.

When one dimension is strongly confined by a tight harmonic oscillator of frequency  $\omega_\perp$ , such that the atoms

occupy only the groundstate along this dimension, an effective two-dimensional GP equation can be derived [51]:

$$\mu\psi_s = \left(-\frac{\hbar^2}{2M}\Delta_s + \frac{\hbar\omega_\perp}{2} + V_s + \frac{g}{\sqrt{2\pi}\sigma}|\psi_s|^2\right)\psi_s,$$

where  $\psi_s$ ,  $\Delta_s$ ,  $V_s$  are the wavefunction, Laplacian and potential, restricted onto the surface, respectively, and  $\sigma = \sqrt{\hbar/(M\omega_\perp)}$  is the length scale associated to the transverse confinement  $\omega_\perp$ .

Since we neglect here all curvature effects, we may connect directly this equation with the notations of the main text:

$$\begin{aligned} \mu\psi_s = & -\frac{\hbar^2}{2M} \frac{1}{r_s(\theta)^2 \sin\theta} \frac{\partial}{\partial\theta} \left( \sin\theta \frac{\partial\psi_s}{\partial\theta} \right) \\ & + \left( V_{2D}^{\text{Fl}}(\theta) + \frac{g}{\sqrt{2\pi}\sigma(\theta)} |\psi_s|^2 \right) \psi_s, \end{aligned}$$

where  $V_{2D}^{\text{Fl}}(\theta) \equiv V(r_s(\theta), \theta) + \hbar\omega_\perp(\theta)/2$ . We then obtain the Thomas-Fermi solution by neglecting the kinetic energy term resulting in:

$$|\psi_s|^2 = \frac{\sqrt{2\pi}\sigma(\theta)}{g} (\mu - V_{2D}^{\text{Fl}}(\theta)).$$

As shown in the main text this simple form captures the main features of the dimensional reduction.